A Triboelectric-Nanogenerator-Based Gas–Solid Two-Phase Flow Sensor for Pneumatic Conveying System Detecting

11 authors, including:

Wang Yan
Dalian Maritime University
7 PUBLICATIONS **23** CITATIONS

Taili Du
Dalian Maritime University
6 PUBLICATIONS **5** CITATIONS

Minyi Xu
Dalian Maritime University
85 PUBLICATIONS **1,085** CITATIONS

A Triboelectric-Nanogenerator-Based Gas–Solid Two-Phase Flow Sensor for Pneumatic Conveying System Detecting

Yan Wang, Dehua Liu, Zhiyuan Hu, Tianyu Chen, Ziyi Zhang, Hao Wang, Taili Du, Steven L. Zhang, Zhiqiang Zhao, Tongming Zhou, and Minyi Xu*

The particle concentration and the mass flow rate are the most important parameters describing the gas–solid two-phase flow. Herein, a novel method based on triboelectric nanogenerator is proposed for measuring a particle concentration and the mass flow rate in a gas–solid two-phase pipe flow. The as-fabricated gas–solid two-phase flow triboelectric nanogenerator (GS-TENG) consists of one acrylic base plate, one copper electrode, and one stripe of polytetrafluoroethylene (PTFE) membrane. Different materials can be detected by the GS-TENG, including organic material, such as flour, and inorganic materials, such as copper and soil. PTFE surface morphology is modified to improve the output performance of the GS-TENG in the experiments in order to detect the output electrical signal more efficiently. The peak output current generated by the gas–solid two-phase flow in the GS-TENG shows a mostly linear relationship with the concentration and mass flow rate. In addition, the transferred charge in the process of the flow also shows a highly linear relationship with the concentration and the mass flow rate, which is consistent with the theoretical derivation for the single electrode TENG. The experimental results demonstrate that the measurement error of the GS-TENG is less than 2%.

1. Introduction

Pneumatic conveying system is a typical gas–solid two-phase flow system and has a wide range of industrial applications, such as electric power generation, chemical synthesis, food

Y. Wang, D. Liu, Z. Hu, T. Chen, Z. Zhang, Prof. H. Wang,
Prof. T. Du, Prof. M. Xu
Marine Engineering College
Dalian Maritime University
Dalian 116026, China
E-mail: xuminyi@dlmu.edu.cn
Prof. T. Zhou
School of Civil
Environmental and Mining Engineering
The University of Western Australia
Perth, WA 6009, Australia
Dr. S. L. Zhang
Robotic Materials Department
Max Planck Institute for Intelligent Systems
70569 Stuttgart, Germany
Z. Zhao
Maritime College
Guangdong Ocean University
Zhanjiang 524088, China

The ORCID identification number(s) for the author(s) of this article can be found under https://doi.org/10.1002/admt.202001270.

processing, steel making, metallurgical production, machinery manufacturing, medicine manufacturing, etc.[1,2] Measurements of the particle concentration and the mass flow rate in these processes are critical in investigating the mechanism of the gas–solid flow, optimizing the control of the process, and improving the production efficiency.[3] Pneumatic conveying of powders is a typical application of the gas–solid two-phase flow, where mass flow optimization is very important, especially for the transport system of pulverized fuel or industrial raw materials in a power plant or in a metallurgical plant. It is highly desired to measure the mass flow rate and the particle concentration of pulverized fuel and industrial raw materials in the pipes into the burners or other devices for improving combustion efficiency as well as reducing emissions.[4,5] In addition, the sudden changes in the concentration or mass flow rate of the gas–solid two-phase flow often indicate abnormalities in the conveying equipment. A low conveying mass flow rate makes particle flow unsteady and complicated, especially for the dense-phase pneumatic conveyance. On the other hand, a high conveying mass flow consumes more energy and causes serious pipe abrasion and particle breakup.[6] Therefore, an optimized conveying mass flow rate is crucial in the pneumatic conveying system. It is highly desired to monitor the mass flow, and alerts in time when the mass flow fluctuates in a large range.

There are many methods to measure two-phase flow, such as capacitance method, pressure drop method, ultrasonic method, optical method, acoustic emission method, radiation method, microwave method, electrostatic method, etc.[7–12] However, the measurement accuracy of these methods mentioned above is normally affected by the temperature of the fluids. The particle accumulation on the surface of these sensors will also reduce their accuracy. In addition, the measurement probes utilized in most gas–solid two-phase flow share the common disadvantages due to space effects and wear. Therefore, it is necessary to explore new gas–solid two-phase flow techniques with robust and high durability performance.

In recent years, triboelectric nanogenerator (TENG) based on the triboelectrification effect and electrostatic induction has been developed for energy harvesting and self-powered sensing.[13–23] The electrostatic charges are generated on the surfaces of two dissimilar materials when they are brought into

**ADVANCED
SCIENCE NEWS**
www.advancedsciencenews.com

**ADVANCED
MATERIALS
TECHNOLOGIES**
www.advmattechnol.de

contact. The contact-induced triboelectric charges can generate a potential drop when the two materials are separated, which can drive electrons to flow between the two electrodes built on each surface. Previous studies revealed that triboelectric charge generation can take place in solid–solid interface,[24–27] solid–liquid interface,[28–30] and solid/liquid air interface[31] without exception. Researchers have proposed and investigated U-tube TENG for harvesting water-wave energy,[32] droplet-based electricity generator,[33,34] TENG wave sensor,[35] and U-shaped TENG pressure sensor based on the solid–liquid triboelectrification.[36] In these studies, liquid–solid interfacing TENGs have exhibited extraordinary advantages, including structural simpleness, low cost, robustness, and expandability. When the gas accompanied by dust flows uniformly through the sensor, the physical properties including the flow characteristics (e.g., Reynolds number), chemical properties, and other related parameters of the gas–solid two-phase flow are similar to those of a uniform and homogeneous medium liquid flow in a circular tube. Thus, in this work, we systematically investigated the electrification between gas–solid two-phase flow and solid membrane. Even though the electrification of gas–solid and solid membrane properties is similar to the liquid–solid electrification, the gas–solid contact electrification has yet to be studied. For example, when a liquid contacts the surface of the dielectric material, there are only traces of hydrogen ions and hydroxide ions in pure water because the electron transfer dominates the generation of contact electrification charges. Transferred charge is primarily caused by electron transfer, and ion transfer is a minority effect according to the results of Nie et al.[37] Whether a similar charge transfer process will occur between the gas–solid two-phase flow and solid is needed to be investigated.

In this study, a gas–solid two-phase flow triboelectric nanogenerator (GS-TENG) based on contact electrification of gas–solid two-phase flow and solid is investigated. It is also developed to measure the concentration or mass flow rate of gas–solid two-phase flow and to monitor the variation of these parameters. An alarming signal will then be sent out when the concentration exceeds a critical value. A simple structure, low cost, and self-powered gas–solid two-phase flow sensor is designed in this work to evaluate the contact electrification between gas–solid and solid. Light weight (0.91 g), thin thickness (0.9 mm), and negligible cost are the characteristics of the

GS-TENG. Universal applicability for more gas–solid two-phase flow types, high detection accuracy on high concentration gas–solid two-phase flow, low installation accuracy, well exchangeability, and high temperature adaptability are the advantages of the GS-TENG compared to the other gas–solid two-phase flow sensor. The GS-TENG is made of an acrylic base plate, copper electrode, and polytetrafluoroethylene (PTFE) membrane. The working mechanism of the GS-TENG is similar to that of a liquid–solid interfacing TENG and its mechanism of the power generation is derived and clarified in Section 2.1. A simplified circuit model is designed to demonstrate the effectiveness of the GS-TENG. In Section 2.2, the angle between the GS-TENG and the ingredient of the gas–solid two-phase flow on the sensitivity of the electric signal are studied and analyzed. Surface morphology treatment is the normal method to improve the output performance of the TENG. The effect of the surface finishing on the output performance is examined. In addition, the organic matter (flour) as well as the inorganic materials (copper and soil) can be detected by the GS-TENG. In Section 2.3, concentration measuring and alarm experiments are conducted to demonstrate the application of the GS-TENG.

2. Results and Discussion

2.1. Structure and Working Principle of the GS-TENG

Figure 1a illustrates the application of the GS-TENG in the pipeline pneumatic conveying system for the transportation of industrial materials. The solenoid valve on the branch line opens every once in a while, and the main line is closed, that is when the GS-TENG measures the gas–solid two-phase flow. The gas–solid two-phase flow contacts the surface of the GS-TENG during the transportation of the material. This is how continuous sampling detection can be realized. As shown in the Figure 1b, the GS-TENG is made of one acrylic base plate, one copper electrode and one stripe of PTFE membrane. To construct the GS-TENG, an acrylic plate with a diameter of 3 cm is used as the base. Copper tape is attached to the base plate as the electrode. Commercial PTFE membrane (with a thickness of 50 µm) is used to cover the surface of the copper electrode as shown in the Figure 1c. In addition, the PTFE surface is treated in order to enhance the electrification effect in the
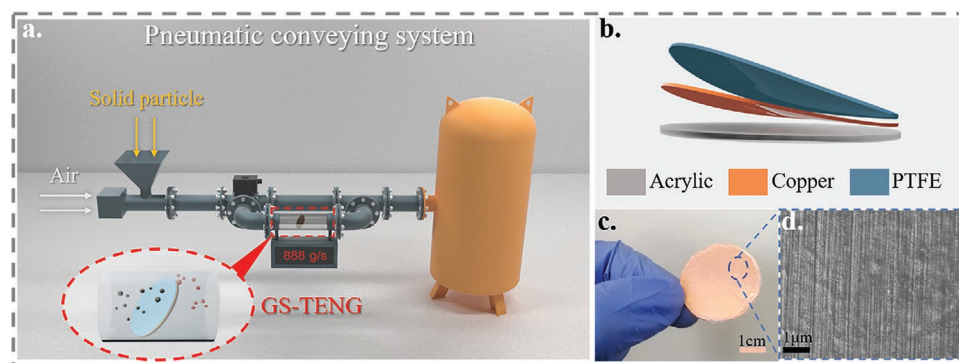

Figure 1. a) Schematic diagram of the working status of the GS-TENG in pipeline. b) Schematic diagram of the GS-TENG. c) The image of the as-fabricated GS-TENG. d) SEM image of the treated PTFE surface.
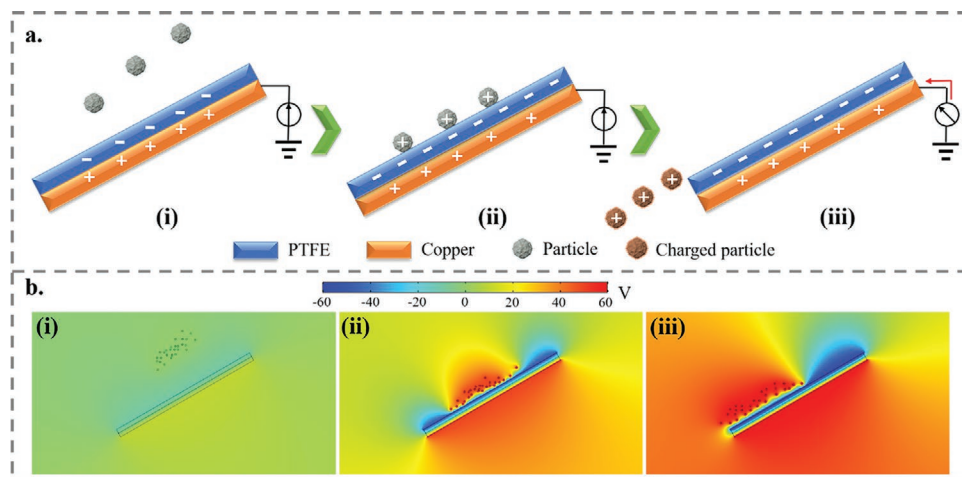
**ADVANCED
SCIENCE NEWS**

www.advancedsciencenews.com

**ADVANCED
MATERIALS
TECHNOLOGIES**

www.advmattechnol.de

Figure 2. Working mechanism of the GS-TENG. a) Schematic diagram for the working principle of GS-TENG. b) Simulations of electric potential distributions for the GS-TENG.

gas–solid two-phase flow, with the scanning electron microscopy (SEM) image shown in Figure 1d. The morphology of the PTFE surface before and after treatment is shown in Figure S1, Supporting Information.

Figure 2a illustrates the detailed working principle of the GS-TENG. PTFE is a polymer dielectric material with high electronegativity. As a good electret, when the gas–solid two-phase flow passes through the PTFE on the sensor surface, electrons can stay there for 1–2 days or even longer, so the PTFE can be treated as a capacitor.[38] The PTFE membrane is pre-charged when the surface is sanded treat. The amount of the positive charges on the copper electrode equals to the negative charges on the PTFE before the particle contacts the PTFE due to the electrostatic induction effect. As a result of contact electrification, when the particle contacts the PTFE surface, the particle becomes positively charged while the PTFE becomes more negatively charged. After the positively charged particles slide off the PTFE surface, it disables the copper electrode with positive charges to screen the more negatively charged PTFE. Therefore,

a flow of current between the ground and copper electrode is induced by the electrostatic induction. The charging and discharging of the copper electrode is realized by draining current from the ground, which is quite similar to the working mechanism for a single electrode TENG.[39,40] To clearly demonstrate the working principle of the GS-TENG, the electric potential distributions of the corresponding states are simulated by COMSOL Multiphysics software as shown in Figure 2b. The models used in the COMSOL simulation software are AC/DC modules. The distribution of the instantaneous electric field of the GS-TENG is calculated, and the geometry parameters of the simulated model are consistent with real device.

The PTFE membrane and copper electrode form a balanced system as shown in the **Figure 3**a. To illustrate the generating of charge clearly, the equivalent topology of the GS-TENG is set here. The entire system for the GS-TENG can be simplified as a physical model with three capacitors refer to the work of Nie et al.,[34] as shown in Figure 3b. When the particle slides off with the PTFE, the charges on the particle, balanced system,
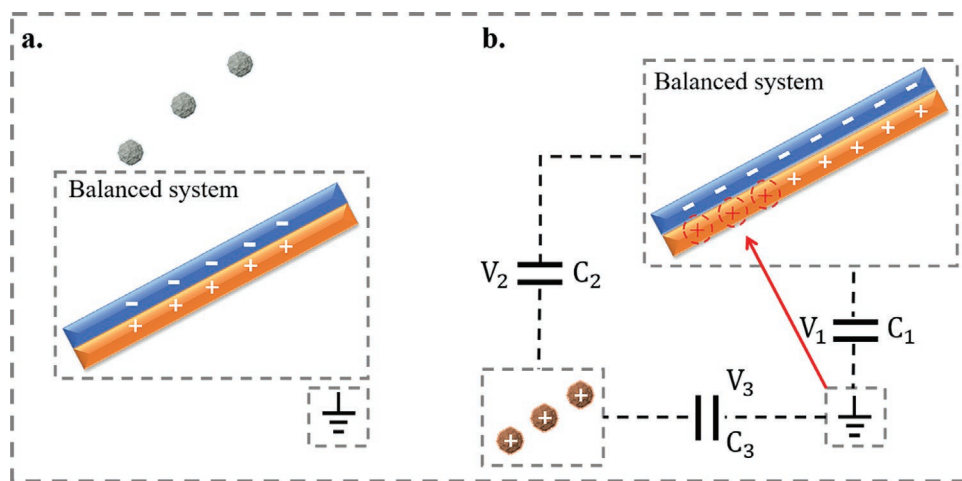

Figure 3. Physical model of the GS-TENG. a) Schematic diagram of the balanced system. b) Circuit model with three capacitances for gas–solid two-phase flow.

**ADVANCED
SCIENCE NEWS**
www.advancedsciencenews.com

**ADVANCED
MATERIALS
TECHNOLOGIES**
www.advmattechnol.de

and ground are q, $-q$, and 0, respectively. Meanwhile, a capacitance exists between the particle and ground. When the system is in an open circuit condition, based on the basic characteristics of capacitance and charge conservation at each position, the following equation can be used to describe the relationship between V_i (i = 1, 2, 3) and corresponding C_i (i = 1, 2, 3). As the air among the particle, GS-TENG and the ground is equivalent to a capacitance, according to the capacitance current equation

$$V_3 = V_1 + V_2 \tag{1}$$

$$-C_1 \frac{dV_1}{dt} + C_2 \frac{dV_2}{dt} = -I_1 + I_2 \tag{2}$$

$$-C_1 \frac{dV_1}{dt} + C_2 \frac{dV_2}{dt} = -I_1 + I_2 \tag{3}$$

$$\int (I_3 + I_2) \, dt = q(t) \tag{4}$$

$$\int (-I_1 + I_2) \, dt = -q(t) \tag{5}$$

According to the integral equation, the maximum open circuit voltage V_{OC} can be obtained with the following equations

$$V_{OC} = V_1 = \frac{qC_3}{C_1 C_2 + C_2 C_3 + C_1 C_3} \tag{6}$$

$$V_{OC} = V_1 = \int \frac{I_1 - I_2}{C_1} \, dt + \frac{C_2}{C_1} \left(\int \frac{I_3 + I_2}{C_2} \, dt - \frac{C_3}{C_2} V_3 \right) \tag{7}$$

$$V_{OC} = V_1 = \frac{q(t)}{C_1} + \frac{C_2}{C_1} \left(\frac{q(t)}{C_2} - \frac{C_3}{C_2} V_3 \right) \tag{8}$$

When the distance between the PTFE and particle is infinity, the value of C_2 and C_3 is close to 0, whereas the ratio C_2/C_3 is close to 1, and V_3 is close to 0. Thus, the maximum V_{OC} and I_1 can be obtained as

$$V_{OC} \approx \frac{q}{2C_1} \tag{9}$$

$$I_1 \approx 2 \frac{dq(t)}{C_1 dt} \tag{10}$$

The particles contacting with the PTFE result in the transferred charge and current flow between the copper electrode and ground. The higher concentration of the particles in the gas–solid two-phase flow represents more particles and more transferred charge. According to Equation (10), the output current of the GS-TENG has a mostly linear relationship with the transferred charge in a certain period of time ($\frac{dq(t)}{dt}$). The magnitude of the current can be represented by the transferred charge. Thus, the output current of the GS-TENG represents the concentration of the gas–solid two-phase flow as indicated by Equation (10). This is the critical feature that the concentration measurement with a GS-TENG is based upon.

2.2. Performance of the GS-TENG

The status of gas–solid two-phase flow in the pipe is displayed in Movie S1, Supporting Information. Powders in the flow are assumed to be evenly distributed, while the pneumatic conveying velocity is set to 9 m s⁻¹. It can be observed that the surface morphology of the PTFE is an important factor that affects the performance of the GS-TENG. The sanded PTFE surface is lumpier and has more grooves, as shown in Figure S1b, Supporting Information. When the particles interact with the PTFE membrane, the microstructures on the PTFE membrane can greatly increase the contact area with the PTFE membrane, which effectively improves the performance of the GS-TENG.[41,42] The width of the grooves is less than 0.1 μm, which is much smaller than the particle diameter (about 75 μm). Thus, there is no possibility of particles embedding in the grooves. Electrostatic adsorption phenomenon occurs when a large voltage field exists. Dust can be absorbed by the electrostatic at the voltage of 1000 V according to the results of Chen et al.[43] The voltage generated by the GS-TENG is much smaller than that value. Furthermore, Previous works indicate that the treated PTFE has the outstanding performance of hydrophobicity and a low coefficient of friction.[35,44,45] Hence, dust is difficult to adhere to the PTFE surface. In addition, maintenance is essential to make pneumatic conveying system working normally and efficiency. Clean the PTFE surface regularly to ensure the accuracy and sensitivity of detection. By treating the surface of the PTFE, the output current and transferred charge of the GS-TENG (as shown in Figure S2a,b, Supporting Information) is increased drastically from 0.008 μA and 1.8 nC to 0.35 μA and 82 nC.

The angle (α) between the surface of the GS-TENG and radial direction of the pipeline is another critical parameter in the two-phase flow measurement in that α is relevant to the energy conversion efficiency and the effective contact area. **Figure 4**a shows the working state of the GS-TENG. Copper particles in the air are utilized in the experiment. When the copper particles contact and slide on the PTFE surface, they lose their electrons and the PTFE absorbs the same amounts of electrons, thus charge is generated on the copper particle. The copper electrode on the other side of the PTFE absorbs the electrons from the ground to balance the potential difference caused by the negative charge on the PTFE surface. The angle (α) can be adjusted by rotating the shaft in the GS-TENG as shown in Movie S1, Supporting Information. Figure 4b shows the current for particles passing through the GS-TENG. It can be observed that a higher concentration of the gas–solid two-phase flow results in a higher output current, as higher concentration means more particles in the flow, and more charges transferred. Similar results can be obtained when the angle (α) is changed (as shown in Figure 4c–e). With increasing α, the electrical signal shows an increasing trend first and then decreasing. A peak output current of 0.98 μA is obtained with α = 45° when the particle concentration is 8000 g m⁻³. Figure 4f shows the linear relationship between the concentration and the peak output current at different angles, which is also consistent with Equation (10). The slope of the data measured with α = 45° is higher than that with other angles, indicating the higher sensitivity and higher energy conversion efficiency

ADVANCED
SCIENCE NEWS
www.advancedsciencenews.com

ADVANCED
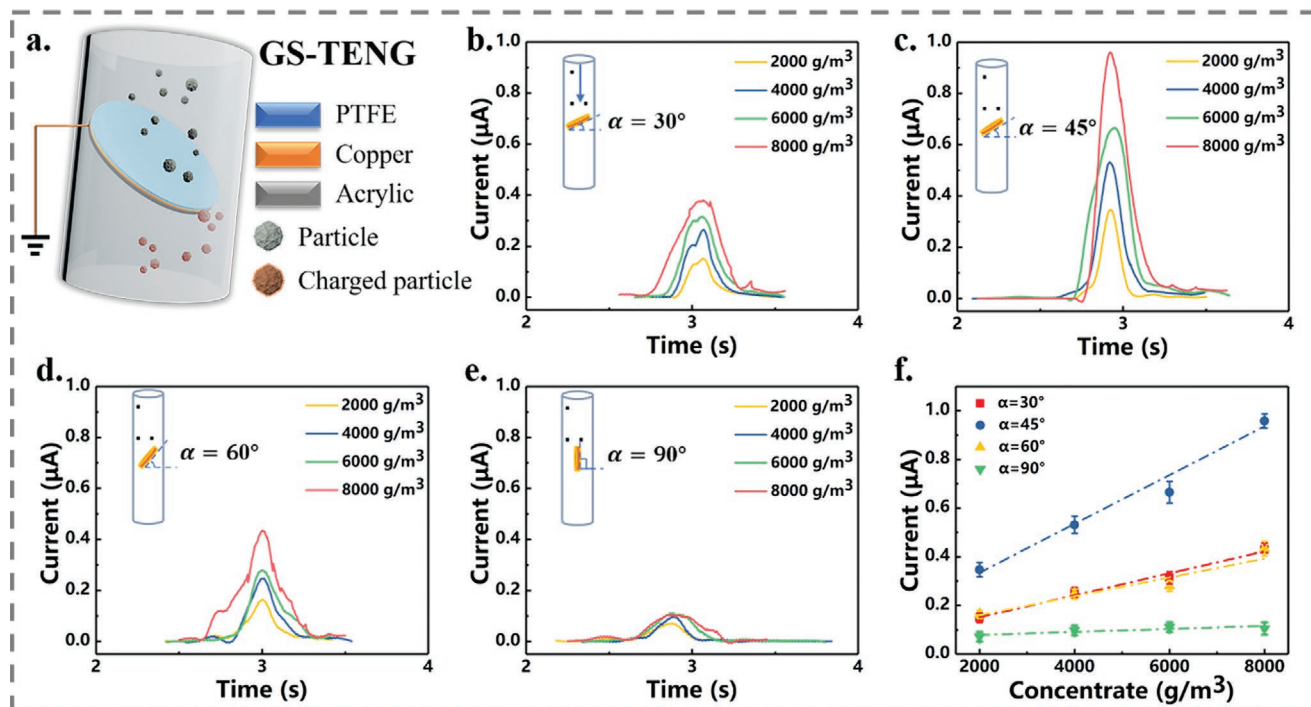MATERIALS
TECHNOLOGIES
www.advmattechnol.de

Figure 4. Variation of the output current of the GS-TENG with respect to the angle and the concentrate ratio of the gas–solid two-phase flow. a) Schematic diagram of GS-TENG in the pipe. b) Output current of the GS-TENG when $\alpha = 30°$. c) Output current of the GS-TENG when $\alpha = 45°$. d) Output current of the GS-TENG when $\alpha = 60°$. e) Output current of the GS-TENG when $\alpha = 90°$. f) Variation of the peak current with respect to the flow angle when $\alpha = 30°–90°$.

of the GS-TENG at this angle. Our results are consistent with those reported by Liu et al.[45] and Gu et al.[46] Dust particles are found to carry positive charges, and the amount of charge it carried is on the order of 10^{-16} C.[47] The amount of charge carried by particles is much lower than the transferred charge of the GS-TENG, so it will hardly affect the accuracy of the GS-TENG.

In order to confirm whether the GS-TENG has the ability to detect different kinds of gas–solid two-phase flow, organic (flour) and inorganic (copper and soil) materials are used as the solid components, respectively, and the angle (α) is set to 45°. **Figure 5**a shows the output current measured by the GS-TENG for the different concentration of pulverized copper (ranging from 400 to 6000 g m^{-3}). This range is determined by referring to the coal-dust mass flow of typical coal-fired power stations.[48] A clear gradient of peak output current is shown in the Figure 5a, and the peak output current increases from 0.02 to 0.66 µA when the concentration increases from 400 to 6000 g m^{-3}. For the flour flow, the peak output current increases from 0.004 to 0.11 µA when the concentration increases from 400 to 6000 g m^{-3} as shown in Figure 5b. It is interesting to note that the output current of the soil flow is negative (Figure 5c). This can be explained by the complex composition of soil: as the soil particles may absorb the electrons and the PTFE membrane lose electrons when the soil particles slide on the PTFE surface. In that case, positive charges flow to the ground from the copper electrode due to the electrostatic induction. Thus, the output current generated by the soil flow is negative. Figure 5d shows the transferred charge for different concentration of the pulverized copper flow. More charges can be transferred for more concentrated pulverized copper flow.

The transferred charge for pulverized copper flow reaches 90 nC when the concentration is 6000 g m^{-3}, which is about twice of that of the flour and soil flow at the concentration of 6000 g m^{-3}, as shown in Figure 5e,f. As the pneumatic conveying velocity and diameter of the pipe are constant, the mass flow rate (M) of the gas–solid two-phase flow can be calculated as $M = \frac{\pi D^2}{4} UC$, in which D is the diameter of the pipe, U is the pneumatic conveying velocity, and C is the concentration of the particle in the gas–solid two-phase flow. As a result, the relationship between the corresponding mass flow rate of the gas–solid two-phase flow and the output current is shown in the Figure 5g–i. For the quality assurance of this study, the reliable tests are performed in 3 days. It turns out that the device output current is almost consistent when the input concentration is 6000 g m^{-3} for the pulverized copper flow as shown in Figure S3, Supporting Information. As shown in Figure S4, Supporting Information, the output current keeps constant in continuous operation of 17 cycles, confirming superior stability of the GS-TENG.

2.3. Demonstrations of the GS-TENG

Demonstration experiments to illustrate the application of the GS-TENG for concentration monitoring and alarming are conducted and the results are shown in **Figure 6**. The program is designed to measure the concentration of the gas–solid two-phase flow according to the linear relationship between the output peak current and the concentration as shown in the diagram of the Figure 6a(i),b(i). The LabVIEW software is used to
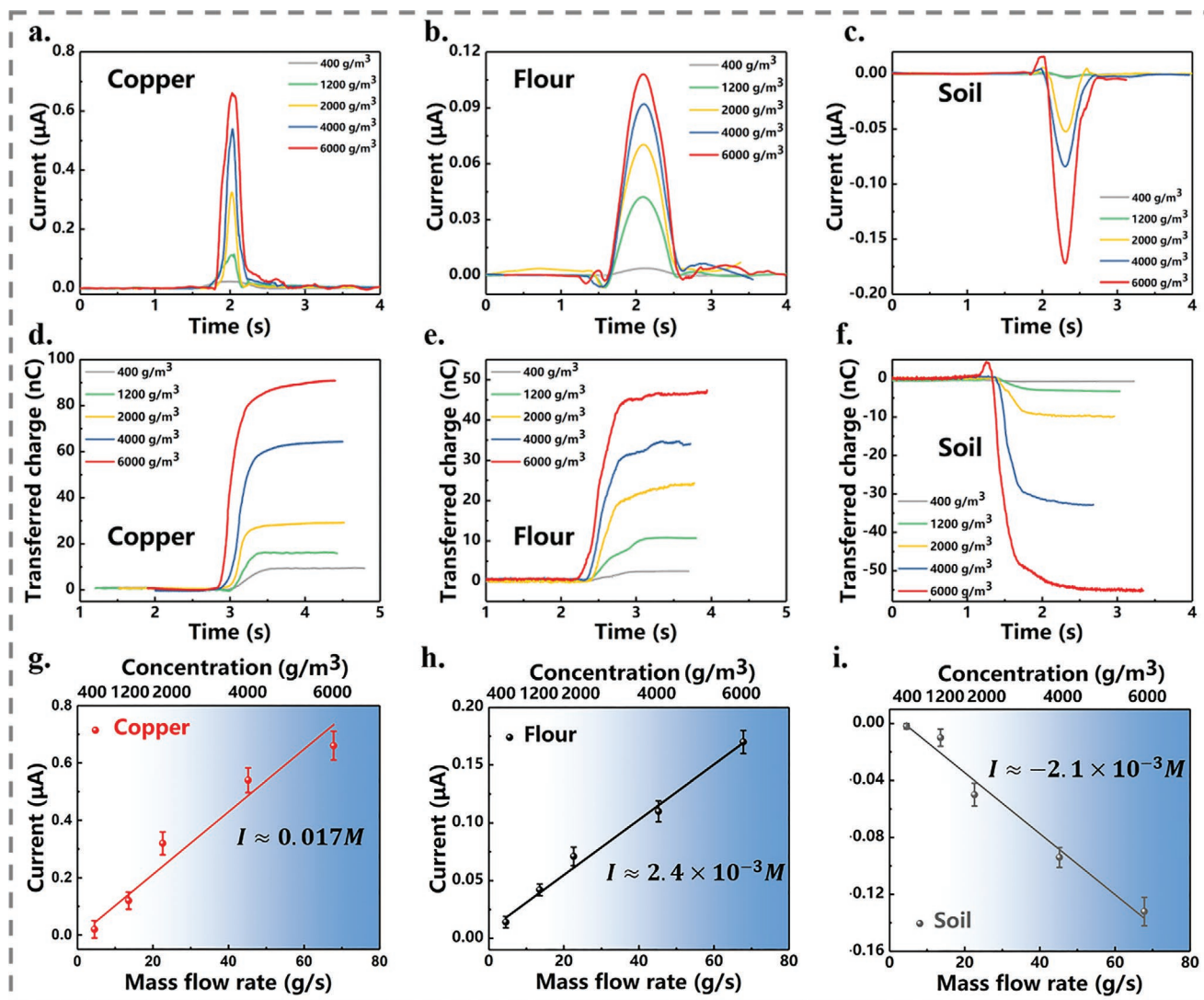
**ADVANCED
SCIENCE NEWS**

www.advancedsciencenews.com

**ADVANCED
MATERIALS
TECHNOLOGIES**

www.advmattechnol.de

Figure 5. The output current and transferred charge measured with different ingredients. a) Comparison of the GS-TENG's output current with different concentration of pulverized copper flow. b) Comparison of the GS-TENG's output current with different concentration of flour flow. c) Comparison of the GS-TENG's output current with different concentration of soil flow. d) Comparison of the GS-TENG's transferred charge with different concentration of pulverized copper flow. e) Transferred charge comparison with different concentrations of flour flow. f) Comparison of the transferred charge with different concentration of soil flow. Output current versus mass flow rate and concentration (not to scale) of g) copper powder; h) flour; and i) soil.

design a program and interface as shown in Figure 6a(ii),b(ii). As the concentration of the particle in the gas–solid two-phase flow has a linear relationship with the peak output current, the GS-TENG provides a feasible way to measure the concentration and mass flow rate of the gas–solid two-phase flow. Figure 6a(i) shows the diagram of the GS-TENG for the concentration measurement. In the demonstration experiment, the concentration of the copper powder is obtained using the relationship between the peak output current (I) and concentration (C), i.e., $C = a \cdot I$, where a is a constant coefficient (here $a = 8110.3$). The concentration signal is sent to a computer as presented in Figure 6a(ii) and Movie S2, Supporting Information. Figure 6a(ii),(iii) depicts the continuous sampling tests. When the input copper powder concentration is 1400 and 2200 g m^{-3}, respectively, there is an obvious difference in the peak output current signal as shown in Figure 6a(iii). It is

worth mentioning that the GS-TENG shows high sensitivity in the experiments. The error of the two detections does not exceed 2%, which is close to the deviation of the active charging and detecting methods.[48]

Another demonstration test is done for monitoring the solid concentration in the two-phase flow. Figure 6b(i) shows the diagram of the GS-TENG designed for high concentration alarm. The concentration signal is sent to a computer, as presented in Figure 6b(ii). As shown in Figure 6b(ii) and Movie S3, Supporting Information, when the input copper powder concentration reaches or exceeds a critical value, such as 2000 g m^{-3}, the alarm indicator is activated as shown in Figure 6b(iii). When the input copper powder concentration is 1500 and 1200 g m^{-3}, respectively, the alarm is not activated. Similarly, the GS-TENG can also be extended to realize a low concentration for a gas–solid two-phase flow. The sensitivity of the GS-TENG can reach
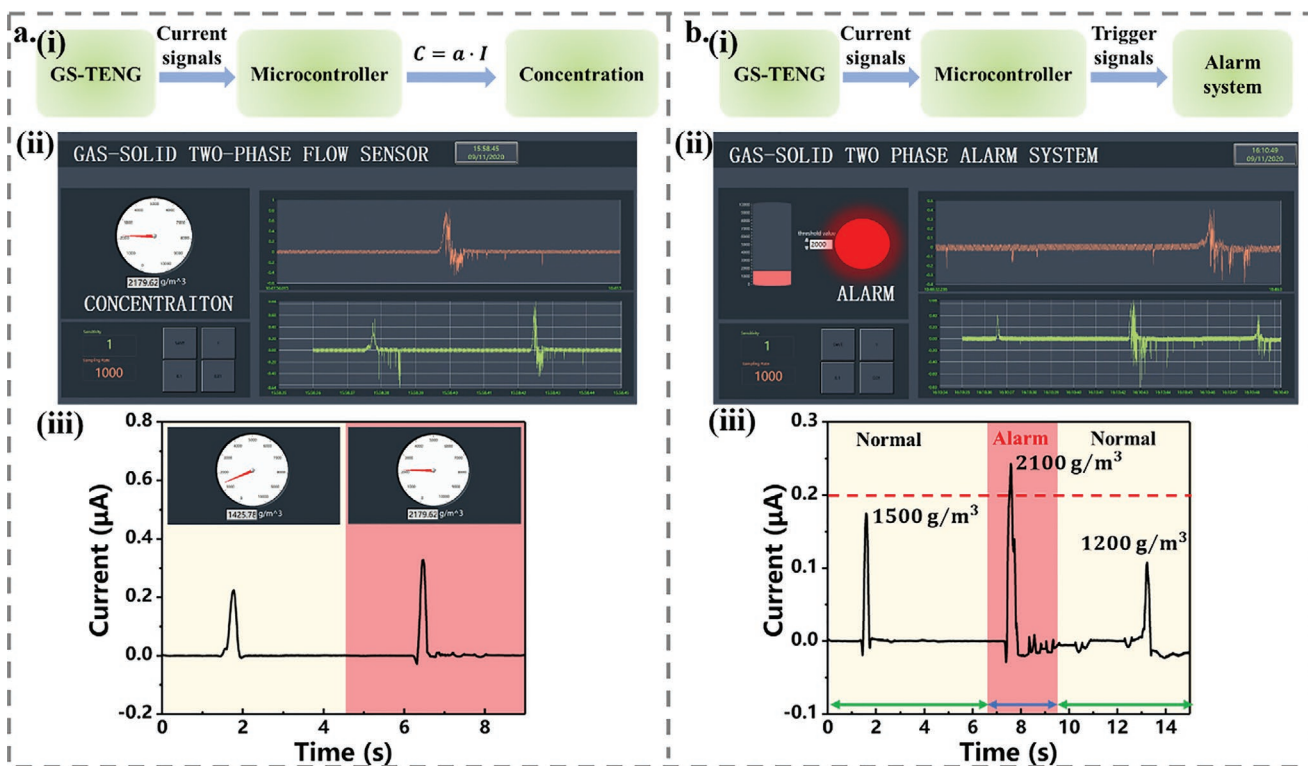
**ADVANCED
SCIENCE NEWS**
www.advancedsciencenews.com

**ADVANCED
MATERIALS
TECHNOLOGIES**
www.advmattechnol.de

Figure 6. Demonstration of the GS-TENG. a) Continuous sampling detection of the GS-TENG. b) Self-powered high-concentration alarm of the GS-TENG.

two decimal places. It can meet the testing needs of pneumatic conveying systems. The surface micro-treatment and strong electronegativity materials can improve the output performance and the accuracy of the GS-TENG. Improved signal processing method, such as connecting amplified and filter module in the external circuit, can improve the sensitivity of the GS-TENG in the future.

3. Conclusion

This study has successfully developed a TENG-based sensor that can measure the concentration and mass flow rate of the gas–solid two-phase flow. A linear relationship is found between the concentration (or mass flow rate) and the peak output current. It is observed that different kinds of gas–solid two-phase flow have different electrical output signal characteristics from the interaction of the GS-TENG. According to this feature, organic matter (flour and soil) and inorganic (copper) materials have been successfully detected in the experiments, which indicate that the GS-TENG has universal applicability. The experiments also reveal that the output current signals of the GS-TENG reach a maximum strength when the interaction angle is 45° and that the treatment of PTFE surface morphology can greatly improve the output performance of the GS-TENG. It is quite impressive to find that the peak current of the GS-TENG with treated PTFE surface morphology can be increased by 40 times of the peak current with the original PTFE surface. In the demonstration experiments for concentration measurement and

high concentration alarming, the GS-TENG shows the characteristics of high sensitivity and high accuracy: the errors of the GS-TENG's measurement are less than 2%. The as-fabricated GS-TENG proves to be quite reliable as a gas–solid two-phase flow sensor. What is more, on observation of its working mechanism, the GS-TENG can be extended to detect the particle concentration in the atmosphere.

4. Experimental Section

Fabrication of the GS-TENG: The fabrication of the GS-TENG is shown in Figure 1b. The PTFE tape (with thickness of 50 µm), the copper electrode, and the acrylic plate were used to fabricate the GS-TENG. The surface of the PTFE membrane was sanded ten times with 10 000 mesh sandpaper to form the microstructure. The GS-TENG was fixed with a metal rod of 1 mm in diameter. The integrated device was set in a tube to measure the gas–solid two-phase flow. The angle between the GS-TENG and the flow can be adjusted by rotating the rod. The microstructure of the PTFE membrane can be observed by E3ISPM electron microscope. The output performance of the TENG can be influenced by the morphology of the dielectric material. The surface of PTFE membrane was polished with 1000 mesh sandpaper (size of 6 cm × 6 cm) from Kafuwell Co., Ltd. The PTFE surface was rubbed ten times in one direction. Then, the microstructure on the PTFE surface can be observed by electron microscope.

Electrical Output Measurement: The experiments for the GS-TENG were performed in a tube with a diameter of 40 and 500 mm long. When the fan installed on the container is started, the particles can be fully mixed with air in the container that has a volume of 600 mL as shown in Figure S5, Supporting Information. The concentration of the particle in the gas–solid two-phase flow can be adjusted by changing the mass of the

particle, as the volume of the container is constant. After the particle was fully mixed in the container, the aspirator was started (with the valve on the tube open). The particles flow through the GS-TENG. The pneumatic conveying velocity is 9.0 m s^{-1}. A programmable electrometer (Keithley Model 6514) was used to measure the electrical output of the GS-TENG.

Supporting Information

Supporting Information is available from the Wiley Online Library or from the author.

Acknowledgements

Conflict of Interest

The authors declare no conflict of interest.

Data Availability Statement

Research data are not shared.

Keywords

[1] Y. Van, B. Byrne, J. Coulthard, *Trans. Inst. Meas. Control* **1993**, *15*, 98.
[2] C. G. Xie, A. L. Stott, A. Plaskowski, M. S. Beck, *Meas. Sci. Technol.* **1990**, *1*, 65.
[3] K. Zhe, W. Xiao-Lei, Z. Shu-Jiang, *Flow Meas. Instrum.* **2013**, *30*, 26.
[4] J. Li, C. Xu, S. Wang, *Flow Meas. Instrum.* **2012**, *27*, 104.
[5] J. Zhang, D. Xu, J. Coulthard, C. Xu, S. Wang, *Chem. Eng. Commun.* **2009**, *197*, 192.
[6] C. Liang, C. S. Zhao, X. P. Chen, W. H. Pu, P. Lu, C. L. Fan, *Chem. Eng. Technol.* **2007**, *30*, 926.
[7] M. P. Mathur, G. E. Klinzing, *Powder Technol.* **1984**, *40*, 309.
[8] S. Wu, Q. Lin, Y. Yuen, Y.-C. Tai, *Sens. Actuators, A* **2001**, *89*, 152.
[9] Y. Yan, B. Byrne, S. Woodhead, J. Coulthard, *Meas. Sci. Technol.* **1995**, *6*, 515.
[10] Y. Yan, J. Ma, *Flow Meas. Instrum.* **2000**, *11*, 195.
[11] J. T. W. Kuo, L.-Y. Chang, P.-Y. Li, T. Hoang, E. Meng, *Sens. Actuators, B* **2011**, *152*, 267.
[12] B. Chen, C. Kwok, T.-A. N. Nguyen, Z. Wang, *Adv. Mater. Technol.* **2018**, *3*, 1800175.
[13] Y. Wang, E. Yang, T. Chen, J. Wang, Z. Hu, J. Mi, X. Pan, M. Xu, *Nano Energy* **2020**, *78*, 105279.
[14] M. Xu, T. Zhao, C. Wang, S. L. Zhang, Z. Li, X. Pan, Z. L. Wang, *ACS Nano* **2019**, *13*, 1932.
[15] T. K. Phan, S. Wang, Y. Wang, H. Wang, X. Xiao, X. Pan, M. Xu, J. Mi, *Sensors* **2020**, *20*, 729.
[16] M. Xu, P. Wang, Y. Wang, S. L. Zhang, A. C. Wang, C. Zhang, Z. Wang, X. Pan, Z. L. Wang, *Adv. Energy Mater.* **2018**, *8*, 1702432.
[17] X. Zhang, M. Yu, Z. Ma, H. Ouyang, Y. Zou, S. L. Zhang, H. Niu, X. Pan, M. Xu, Z. Li, Z. L. Wang, *Adv. Funct. Mater.* **2019**, *29*, 1900327.
[18] X. Cao, Y. Jie, N. Wang, Z. L. Wang, *Adv. Energy Mater.* **2016**, *6*, 1600665.
[19] Y. Xi, H. Guo, Y. Zi, X. Li, J. Wang, J. Deng, S. Li, C. Hu, X. Cao, Z. L. Wang, *Adv. Energy Mater.* **2017**, *7*, 1602397.
[20] J. Zou, M. Zhang, J. Huang, J. Bian, Y. Jie, M. Willander, X. Cao, N. Wang, Z. L. Wang, *Adv. Energy Mater.* **2018**, *8*, 1702671.
[21] Y. Zi, H. Guo, Z. Wen, M.-H. Yeh, C. Hu, Z. L. Wang, *ACS Nano* **2016**, *10*, 4797.
[22] J. Hu, X. Pu, H. Yang, Q. Zeng, Q. Tang, D. Zhang, C. Hu, Y. Xi, *Nano Res.* **2019**, *12*, 3018.
[23] R. Lei, H. Zhai, J. Nie, W. Zhong, Y. Bai, X. Liang, L. Xu, T. Jiang, X. Chen, Z. L. Wang, *Adv. Mater. Technol.* **2019**, *4*, 1800514.
[24] M. Xu, Y. Wang, S. L. Zhang, W. Ding, J. Cheng, X. He, P. Zhang, Z. Wang, X. Pan, Z. L. Wang, *Extreme Mech. Lett.* **2017**, *15*, 122.
[25] Y. Bian, T. Jiang, T. Xiao, W. Gong, X. Cao, Z. Wang, Z. L. Wang, *Adv. Mater. Technol.* **2018**, *3*, 1700317.
[26] P. Wang, L. Pan, J. Wang, M. Xu, G. Dai, H. Zou, K. Dong, Z. L. Wang, *ACS Nano* **2018**, *12*, 9433.
[27] X. Wang, Z. Wen, H. Guo, C. Wu, X. He, L. Lin, X. Cao, Z. L. Wang, *ACS Nano* **2016**, *10*, 11369.
[28] D. Jiang, Y. Su, K. Wang, Y. Wang, M. Xu, M. Dong, G. Chen, *Nano Energy* **2020**, *70*, 104459.
[29] J. Nie, Z. Ren, J. Shao, C. Deng, L. Xu, X. Chen, M. Li, Z. L. Wang, *ACS Nano* **2018**, *12*, 1491.
[30] G. Chen, X. Liu, S. Li, M. Dong, D. Jiang, *Lab Chip* **2018**, *18*, 1026.
[31] G. Xue, Y. Xu, T. Ding, J. Li, J. Yin, W. Fei, Y. Cao, J. Yu, L. Yuan, L. Gong, *Nat. Nanotechnol.* **2017**, *12*, 317.
[32] L. Pan, J. Wang, P. Wang, R. Gao, Y.-C. Wang, X. Zhang, J.-J. Zou, Z. L. Wang, *Nano Res.* **2018**, *11*, 4062.
[33] W. Xu, H. Zheng, Y. Liu, X. Zhou, C. Zhang, Y. Song, X. Deng, M. Leung, Z. Yang, R. X. Xu, Z. L. Wang, X. C. Zeng, Z. Wang, *Nature* **2020**, *578*, 392.
[34] J. Nie, Z. Wang, Z. Ren, S. Li, X. Chen, Z. L. Wang, *Nat. Commun.* **2019**, *10*, 2264.
[35] M. Xu, S. Wang, S. L. Zhang, W. Ding, K. T. Phan, C. Wang, Z. Li, X. Pan, Z. L. Wang, *Nano Energy* **2019**, *57*, 574.
[36] X. Zhang, Y. Zheng, D. Wang, F. Zhou, *Nano Energy* **2017**, *40*, 95.
[37] J. Nie, Z. Ren, L. Xu, S. Lin, F. Zhan, X. Chen, Z. L. Wang, *Adv. Mater.* **2020**, *32*, 1905696.
[38] L. L. Cui, M. H. Song, Y. X. Kong, L. Cheng, D. Wang, Y. H. Xiao, J. Jiang, *J. Electrostat.* **2009**, *67*, 412.
[39] S. Niu, Y. Liu, S. Wang, L. Lin, Y. S. Zhou, Y. Hu, Z. L. Wang, *Adv. Funct. Mater.* **2014**, *24*, 3332.
[40] P. Bai, G. Zhu, Q. Jing, Y. Wu, J. Yang, J. Chen, J. Ma, G. Zhang, Z. L. Wang, *Nano Energy* **2015**, *12*, 278.
[41] J. Wu, X. Wang, H. Li, F. Wang, W. Yang, Y. Hu, *Nano Energy* **2018**, *48*, 607.
[42] H. Zhao, X. Xiao, P. Xu, T. Zhao, L. Song, X. Pan, J. Mi, M. Xu, Z. L. Wang, *Adv. Energy Mater.* **2019**, *9*, 1902824.
[43] Q. Chen, M. Fang, J. Cen, M. Lv, S. Shao, Z. Xia, *Powder Technol.* **2019**, *345*, 352.
[44] Z. Lin, G. Cheng, S. Lee, K. C. Pradel, Z. L. Wang, *Adv. Mater.* **2014**, *26*, 4690.
[45] X. Liu, A. Yu, A. Qin, J. Zhai, *Adv. Mater. Technol.* **2019**, *4*, 1900608.
[46] G. Gu, C. Han, Y. Bai, T. Jiang, C. He, B. Chen, Z. Wang, *Adv. Mater. Technol.* **2018**, *3*, 1800009.
[47] J. C. Gao, J. G. Zhang, presented at *Proc. of the Forty-Eighth IEEE Holm Conf. on Electrical Contacts* (Eds: M. Braunovic, D. Moore), IEEE, Piscataway **2002**, pp. 191–196.
[48] Y. Yan, *Meas. Sci. Technol.* **1996**, *7*, 1687.